A Phase Filter for Multi-Pass InSAR Stack Data by Hybrid Tensor Rank Representation

YANAN YOU [ID], **(Member, IEEE), RUI WANG** [ID], **(Student Member, IEEE), AND WENLI ZHOU**
Beijing Key Laboratory of Network System Architecture and Convergence, Beijing University of Posts and Telecommunications, Beijing 100088, China

Corresponding author: Rui Wang (wangrui-happy@bupt.edu.cn)

ABSTRACT Multi-pass synthetic aperture radar interferometry (InSAR) stack data denoising is a significant prerequisite for extracting geophysical parameters. InSAR stack data can be considered as a third-order tensor in the complex domain, and the process of tensor decomposition to acquire the low-rank tensor has been employed as an effective interferometric phase filter for InSAR stack data. It is noted that the definition of tensor rank is the core of tensor-based filter. In this paper, we investigate the properties of Tucker rank, CANDECAMP/PARAFAC (CP) rank and Kronecker Basis Representation (KBR) in InSAR stack data, and then we found that it is suitable to extend KBR, as a hybrid tensor rank representation, into InSAR tensor filtering. Firstly, an improved InSAR phase tensor model is utilized to represent the phenomenon of interferometric phase, which perceives the observed InSAR phase tensor as the combination of low-rank, sparse noise and Gaussian noise tensors. Based on the principle of KBR, then the novel phase filtering method, named as KBR-InSAR, is proposed to decompose the complex InSAR tensor supported by the improved InSAR phase tensor model. With the comparison of other tensor filters, i.e. HoRPCA and WHoRPCA and the widespread traditional filters operating on a single interferometric pair, e.g. Goldstein, NL-SAR, NL-InSAR and InSAR-BM3D, it can be proved that the KBR-InSAR can efficiently reduce the noise with superior fringes preservation in the experiments on the simulated and real InSAR stack data collected from Sentinel-1B.

INDEX TERMS Synthetic aperture radar (SAR), SAR interferometry (InSAR), tensor decomposition, KBR, phase filtering.

I. INTRODUCTION

Multi-pass synthetic aperture radar interferometry (InSAR) technique has gained a great achievement on elevation inversion [1] and deformation monitoring [2] by processing InSAR stack data. The elimination of noise in InSAR stack data is a significant prerequisite for extracting geophysical parameters. There are some straightforward approaches, still popular among researchers, focus on filtering on a single interferometric pair. The first attempt to remove phase noise simply averages a fixed-size sliding window (boxcar filter) [3] which has caused an unavoidable loss of resolution. The adaptive filters [4]–[6] are often used in two-dimensional image processing. In fact, in the field of interferometric phase filtering, there are also some adaptive methods. Goldstein filter [7], characterized by construction in frequency domain,

adaptively adjust based on local fringes, but it has the deteriorated performance at the region of dense fringes or high noise intensity [8]. The non-local filter method averages the similar pixels not only around the center pixel but also going through the entire image, including SAR images [9] and polarimetric images [10]. Based on non-local means (NL-means) [11], some filters for interferograms have been proposed with appropriate phase-oriented method, e.g. Non-local InSAR (NL-InSAR) [12]. Furthermore, in order to enhance the robustness of non-local algorithms, a denoising framework for (In)SAR called as Nonlocal SAR (NL-SAR) [13] is proposed to handle the various fringe patterns with adaptive selection of filter parameters, e.g. the size of search window. An improved version of NL-means is proposed relying on the combination of non-local conception and Wiener filter, called as non-local block-matching 3-D (i.e. BM3D) [14]. Researchers extend BM3D to filter the noise in interferogram, which is called as InSAR-BM3D [15],

and that has a good performance in most cases. In general, non-local filters guarantee a good preservation of fringes in phase slowly-changing areas.

Recently, the phase filtering approaches based on tensor decomposition effectively restore the interferograms by using the entire InSAR stack data [16], [17]. In fact, multi-baseline and multi-temporal InSAR stack data is third-dimensional, where the first and second dimension are spatial distribution of an interferogram, and the third dimension denotes the temporal variation of the interferograms, i.e. the number of interferometric pairs. Therefore, InSAR stack data conforms to the mathematical representation of tensor and it has a low rank structure. Although principal component analysis (PCA) [18] can extract this low rank structure, the results obtained by PCA obviously deteriorate because of the existence of the outliers in different interferograms. In order to handle the outliers, robust PCA (RPCA) [19] is proposed to decompose the observed two-dimensional matrix into a low rank matrix and an outlier matrix, however, it destroys the original structure of high-dimensional data, especially for InSAR stack data. In recent years, higher order singular value decomposition (HoSVD) [20] constructs a certain mathematical foundation for the analysis of high-dimensional data. Based on that, higher order RPCA (HoRPCA) which is the promotion of RPCA and HoSVD [21] is proposed and have a great success in image restoration. HoRPCA is first applied to interferometric phase filtering by Kang *et al.* [16], as an effective denoising step in the framework of ground displacement time-series recovery. In this method, InSAR stack data modeled as a tensor can be decomposed into low rank tensor and outlier tensor (i.e. noise in InSAR stack data). Further improvements are proposed in [17], where weighted HoRPCA (WHoRPCA) outperforms by reweighting the low-rank and outlier tensors compared to NL-InSAR and HoRPCA.

The low rank reflects not only the linear correlation within the data, but also the measurement of data sparsity. The clean InSAR stack data is a low-rank tensor, which is because the number of major factors which lead to variation in InSAR stack data is relatively small, and it has been proved in [17]. Therefore, the key to tensor filtering is estimating the low rank tensor. However, due to the correlation between tensor modes, it is a major challenge to define tensor rank in order to obtain low-rank tensor [22]. The main definitions of tensor rank include Tucker rank [20], CANDECAMP/PARAFAC (CP) rank [20] and Kronecker basis representation (KBR) [23] proposed recently. Tucker rank refers to the vector containing the ranks of each mode unfolding of tensor, and it can be relaxed to the sum of the kernel norms of each mode unfolding of tensor for computational convenience, i.e. the sum of nuclear norms [24]. The effectiveness of the relaxation is verified in [25] and [26]. As stated in [16], HoRPCA based on Tucker rank is used for tensor decomposition to obtain the low rank tensor, and this denoising method based on HoRPCA improves the accuracy of extracted geophysical parameters. WHoRPCA in [17] utilizes the same tensor rank

by iterative re-weighting to further improve the estimation accuracy of low rank tensor.

CP decomposition method can decompose a tensor into the sum of Kronecker bases, where the number of Kronecker bases is CP rank. It is worthy to note that CP rank should be predetermined before CP decomposition, which is a challenge for the computation of appropriate CP rank [27]. KBR is composed of two parts: one is the L_0 norm of the core tensor obtained by HoSVD and the other is the product of the ranks of each mode unfolding of tensor. Considering that no published studies using CP rank or KBR to measure the sparsity of InSAR tensor, a sparsity measure of InSAR tensor is analyzed in this paper according to the different definitions of tensor rank, and it is suitable to extend KBR, as a hybrid tensor rank representation, into InSAR tensor filtering.

The previous InSAR phase tensor model in [16], [17] only decomposes a tensor into the low rank tensor and the outlier tensor, the outlier tensor here represents noise in InSAR stack data, and the low rank tensor represents the noise-free interferometric phase. In fact, the interferogram is not only corrupted by the isolated phase jump points caused by spatial under-sampling but also contains additive Gaussian noise (e.g. system thermal noise) [28], [29]. These two types of phase noise have different distribution properties. Therefore, in this paper, firstly, an improved InSAR phase tensor model is utilized to represent the reality of interferometric phase, which perceives the observed InSAR phase tensor as the combination of low-rank, sparse noise and Gaussian noise tensors. Based on the principle of KBR, then the novel phase filtering method, named as KBR-InSAR, is proposed to decompose the complex InSAR tensor supported by the improved InSAR phase tensor model. In our method, KBR is performed separately on real and imaginary parts of InSAR tensor, and iterative optimization with a proper constraint obviously promotes the filter performance.

It can not only prove that KBR-InSAR performs better than other tensor-based filter methods in most cases, but also illustrate that KBR-InSAR has a better preservation of fringes than the filter methods performing on a single interferometric pair in the case of phase with fast-changing by the experiments on the simulated and real InSAR stack data collected from Sentinel-1B.

The rest of this paper is organized as follows. Section II presents some mathematical notations of tensor and preliminaries. Section III briefly introduces Tucker rank and its tensor decomposition method applied in InSAR tensor. Section IV describes CP rank and the limitations of its application in InSAR tensor. Section V elaborates an improved InSAR phase tensor model, and the proposed KBR-InSAR algorithm in detail. Section VI provides experimental results by using the simulated and real data to evaluate the filter performance. Discussions about our method present in Section VII. The conclusion is given in the final part.

II. NOTIONS AND PRELIMINARIES

A. TENSOR

Tensor is the extension of the concept of vector and matrix in multi-dimensional space, which corresponds to a multi-dimensional array. We use boldface capital letters to represent a matrix, e.g. $\mathbf{A}$, and boldface Euler script letters represent a tensor, e.g. $\mathcal{A}$. A tensor can be written as $\mathcal{A} \in \mathbb{R}^{I_1 \times I_2 \times \cdots \times I_N}$, where N represents the order of tensor, and I_n ($n = 1, 2, \cdots, N$) is the size of nth order. Mode-n unfolding of tensor $\mathcal{A}$ is the process of rearranging tensor to a matrix, i.e. $\mathbf{A}_{(n)} \in \mathbb{R}^{I_n \times (I_1 \times \cdots \times I_{n-1} \times I_{n+1} \times I \cdots \times I_N)}$. For example, assuming that $\mathcal{A} \in \mathbb{R}^{I_1 \times I_2 \times I_3}$, and then mode-1 unfolding of tensor $\mathcal{A}$ is $\mathbf{A}_{(1)} \in \mathbb{R}^{I_1 \times I_2 I_3}$.

For $\mathcal{A}_1, \mathcal{A}_2 \in \mathbb{R}^{I_1 \times I_2 \times \cdots \times I_N}$, the inner product of $\mathcal{A}_1$ and $\mathcal{A}_2$ is defined as

$$\langle \mathcal{A}_1, \mathcal{A}_2 \rangle = \sum_{i_1} \sum_{i_2} \cdots \sum_{i_N} \mathcal{A}_1(i_1, i_2, \cdots, i_N)$$
$$\mathcal{A}_2(i_1, i_2, \cdots, i_N) \quad (1)$$

Some norms appear in the following sections, and their definitions are shown as follows. The nuclear norm of a second-order tensor (i.e. a matrix) refers to the sum of the singular values of the matrix, that is

$$\|\mathbf{A}\|_* = \sum_i \sigma_i(\mathbf{A}) \quad (2)$$

where $\sigma_i(\mathbf{A})$ is ith singular value of $\mathbf{A}$. The L_0 norm of a tensor refers to the number of non-zero elements in the tensor, i.e. $\|\mathcal{A}\|_0$. For convenience of calculations, the L_0 norm is always relaxed as the L_1 norm, which denotes as the sum of absolute values of all elements, it is defined as

$$\|\mathcal{A}\|_1 = \sum_{i_1} \sum_{i_2} \cdots \sum_{i_N} |a_{i_1, i_2, \cdots, i_N}| \quad (3)$$

where $a_{i_1, i_2, \cdots, i_N}$ is the element in N-order tensor $\mathcal{A}$. The Frobenius norm refers to the square root of the sum of all tensor elements squares, and is defined as

$$\|\mathcal{A}\|_F = \left(\sum_{i_1} \sum_{i_2} \cdots \sum_{i_N} |a_{i_1, i_2, \cdots, i_N}|^2 \right)^{1/2} \quad (4)$$

Some symbols used in the paper are explained as follows. $\odot$ denotes element-wise product. $\circ$ denotes the vector outer product. $\times_n$ denotes n-mode product, which represents the product of tensor and matrix.

B. InSAR TENSOR MODEL

InSAR stack data is a typical third-order tensor in complex domain [16], and written as $\mathcal{T} \in \mathbb{C}^{I_1 \times I_2 \times I_3}$, where I_1, I_2 represent the spatial distribution of an interferogram, and I_3 denotes the temporal variation of the interferogram, i.e. the number of interferometric pairs.

The noisy InSAR tensor is decomposed into low-rank (information) tensor and outlier tensor (noise). Therefore, the mathematical expression of InSAR phase tensor model is written as

$$\mathcal{T} = \mathcal{L} + \mathcal{E} \quad (5)$$

where $\mathcal{T}$ is the observed InSAR tensor, $\mathcal{L}$ is the low rank tensor and $\mathcal{E}$ is the outlier tensor. Here, $\mathcal{E}$ reflects the phase noise in InSAR stack data.

III. InSAR TENSOR FILTER METHOD BASED ON TUCKER RANK

A. TUCKER RANK

InSAR tensor $\mathcal{T} \in \mathbb{C}^{I_1 \times I_2 \times I_3}$ can be decomposed by HoSVD [20] as (6):

$$\mathcal{T} = \mathcal{S} \times_1 \mathbf{U}_{(1)} \times_2 \mathbf{U}_{(2)} \times_3 \mathbf{U}_{(3)} \quad (6)$$

where $\mathcal{S} \in \mathbb{C}^{P_1 \times P_2 \times P_3}$($P_n < I_n$, $n = 1, 2, 3$) is named as core tensor, $\mathbf{U}_{(n)} \in \mathbb{C}^{P_n \times I_n}$ is an orthogonal factor matrix on the mode-n of $\mathcal{T}$. The low-dimensional approximation of $\mathcal{S}$ can be acquired by the SVD as (7):

$$\mathbf{S}_{(n)} = \mathbf{U}_{(n)} \boldsymbol{\Sigma}_{(n)} \mathbf{V}_{(n)}^H \quad (7)$$

where $\boldsymbol{\Sigma}_{(n)}$ is a diagonal matrix composed of singular values. $\mathbf{V}_{(n)}$ is a column-wise orthonormal matrix, and $(\cdot)^H$ is the conjugate transpose.

It is noted that HoSVD, also known as Tucker decomposition, is influenced by the existence of outliers [21], which unfortunately is a frequent noise in InSAR stack data. Therefore, a series of effective convex optimization frameworks [21], [22] are proposed to handle the outliers by taking the tensor rank as a reference. Tucker rank, used in these frameworks, is a representative method to definite the tensor rank, as shown in (8):

$$Trank(\mathcal{T}) = (r_1, r_2, r_3)$$
$$r_n = rank(\mathbf{T}_{(n)}) \quad (8)$$

where $Trank(\cdot)$ represents Tucker rank of tensor $\mathcal{T}$.

In singleton model, Tucker rank corresponds to the sum of the nuclear norms of all unfolding matrices along all modes, which is successfully used to recover low-rank tensor from noisy tensor in [16], [21] and [30]. Tucker rank can be rewritten as

$$Trank(\mathcal{T}) = \sum_{n=1}^{3} \|\mathbf{T}_{(n)}\|_* \quad (9)$$

The singular value, acquired by the decomposition of matrices whether in real or complex domain, is non-negative and real, and thus Tucker rank of InSAR tensor can be directly calculated by (9).

In order to investigate the property of Tucker rank when applied as the InSAR tensor rank, some noise-free complex InSAR tensors are simulated with the same elevation and deformation model but different ranges of spatial baseline from 50m to 250m, and regarded as tensor group 1 (TG1). The range of spatial baseline is 50m, denoted as the baseline for one interferogram in InSAR tensor randomly distributed in $[-50, 50]$ m. Finally, TG1 contains 9 InSAR tensors.

Then Gaussian noise is added to each tensor in TG1 with the SNR of 5dB, and the outlier ratio is 10%, which means 10% of pixels in each interferogram of tensors
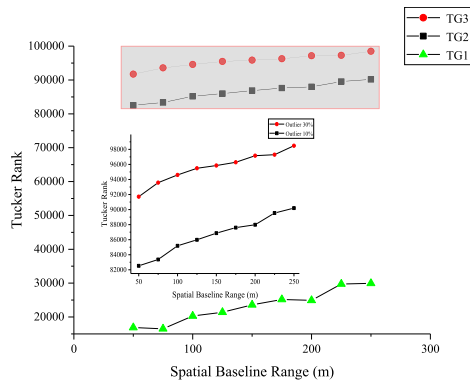
FIGURE 1. Tucker rank of simulated tensor group (TG) 1, 2 and 3. TG1 is a collection of noise-free simulated tensors with different baseline ranges. Spatial baseline range equals x m, denoted that the baseline of an interferogram in InSAR tensor is randomly distributed in [−x, x] m. TG2 is TG1 added 5 dB Gaussian noise and 10% outliers. TG3 is TG1 added 5 dB Gaussian noise and 30% outliers.

in TG1 are randomly set as $-\pi$ or π, and regarded as tensor group 2 (TG2). Tensor group 3 (TG3) is obtained when the outlier ratio is up to 30%. The Tucker rank of each tensor in these TGs is calculated by (9) and shown in Fig. 1.

It can be observed that when Tucker rank is used as the sparsity measure of tensor, the rank of clean InSAR tensor is lower than that of noisy tensor, and it can be inferred that estimating the low rank tensor by Tucker decomposition can achieve the purpose of denoising. In addition, because the correlation for each interferometric pair in InSAR tensor decreases, the Tucker ranks of all TGs increase when the span of spatial baseline grows.

B. HORPCA FOR InSAR TENSOR FILTERING

Based on the model in (5) and Tucker rank, HoRPCA [21], as a classic tensor decomposition method, is introduced to estimate the low rank tensor $\mathcal{L}$ in InSAR tensor. The low-rank problem of tensor decomposition can be modeled as

$$\{\hat{\mathcal{L}}, \hat{\mathcal{E}}\} = \underset{\mathcal{L}, \mathcal{E}}{\arg\min} \, Trank \, (\mathcal{L}) + \lambda \, \|\mathcal{E}\|_0, \quad s.t. \, \mathcal{T} = \mathcal{L} + \mathcal{E} \tag{10}$$

where λ is a regularization coefficient.

The problem in (10) is relaxed as follows, and the effectiveness of the relaxation is verified in [16],

$$\{\hat{\mathcal{L}}, \hat{\mathcal{E}}\} = \underset{\mathcal{L}, \mathcal{E}}{\arg\min} \sum_{n=1}^{3} \left\| \mathbf{L}_{(n)} \right\|_* + \lambda \, \|\mathcal{E}\|_1, \quad s.t. \mathcal{T} = \mathcal{L} + \mathcal{E} \tag{11}$$

The augmented Lagrangian function of (11) is shown as:

$$\begin{aligned} \{\hat{\mathcal{L}}, \hat{\mathcal{E}}\} = \arg\min \sum_{n=1}^{3} \left\| \mathbf{L}_{(n)} \right\|_* + \lambda \, \|\mathcal{E}\|_1 \\ + (\frac{\mu}{2} \, \|\mathcal{L} + \mathcal{E} - \mathcal{T}\|_F^2 - \langle \mathcal{M}, \mathcal{L} + \mathcal{E} - \mathcal{T} \rangle) \end{aligned} \tag{12}$$

where $\mathcal{M}$ is the Lagrangian multiplier updated literately. μ and λ are regularization coefficients. The low-rank tensor
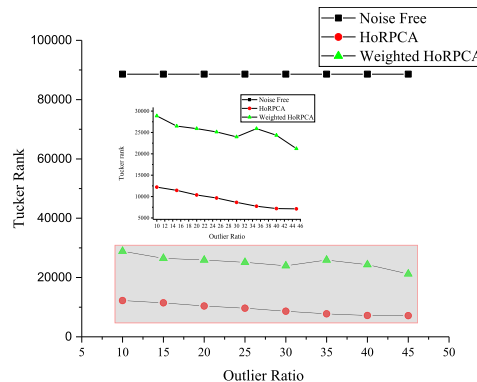
can be obtained by solving (12) and using alternating direction multiplier method (ADMM) [31].

Because that the sparsity of each mode of InSAR tensor is considered in the relaxation of Tucker rank, HoRPCA balances the preservation of fringes and the elimination of noise. However, in some cases, its performance has a serious deterioration, for example, the excessive smoothing will occur when outlier ratio is high.

In order to investigate the property of HoRPCA affected by various outlier ratios in InSAR tensor, one noise-free complex InSAR tensor in TG1 with the spatial baseline range equaled to 250 m is selected, and then the selected InSAR tensor is added Gaussian noise with the SNR of 5dB and different outlier ratios varying from 10% to 45%. The approach to simulate outlier is same as the method used in generating TG2. The Tucker rank of clean InSAR tensor and filtered results acquired by HoRPCA and WHoRPCA is shown in Fig. 2.

As shown in Fig. 2, the Tucker rank of InSAR tensor filtered by HoRPCA decreases continuously when the InSAR tensor is imposed with a higher outlier ratio. However, HoRPCA will be over-smoothed when fringes are dense, which leads to a lower Tucker rank of filtering result than the noise-free InSAR tensor.

C. WHORPCA FOR InSAR TENSOR FILTERING

The convex optimization algorithm in HoRPCA satisfies the requirement of low-rank tensor recovery under most circumstances, but it is subject to the existence of high outlier ratio in the observed InSAR tensor. Therefore, the methods of reweighted low-rank matrix [32] and outlier tensor [33] are utilized to improve the performance of HoRPCA [17], here, the optimization expression is rewritten as

$$\begin{aligned} \{\hat{\mathcal{L}}, \hat{\mathcal{E}}\} = \underset{\mathcal{L}, \mathcal{E}}{\arg\min} \sum_{n=1}^{3} \sum_{j} \left| w_{nj} \sigma_j(\mathbf{L}_{(n)}) \right|_1 + \lambda \, \|\mathcal{W}_{\mathcal{E}} \odot \mathcal{E}\|_1 \\ s.t. \, \mathcal{T} = \mathcal{L} + \mathcal{E} \end{aligned} \tag{13}$$

where w_{nj} is the weight value assigned to the jth singular values of $\mathbf{L}_{(n)}$, $\mathcal{W}_{\mathcal{E}}$ denotes the weight tensor imposed on the outlier tensor.

FIGURE 2. The Tucker rank of the clean InSAR tensor, and the filtered InSAR tensors acquired by HoRPCA and WHoRPCA.
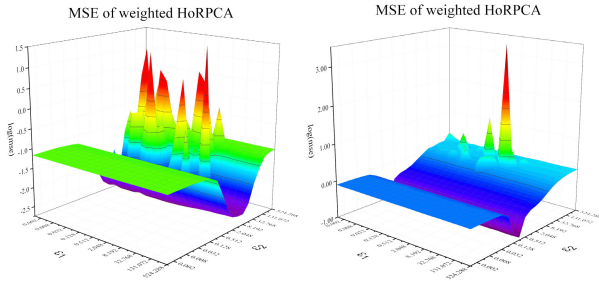
FIGURE 3. MSE between the ideal reference and filtered tensor acquired by WHoRPCA when the parameter pair adjusts. WHoRPCA processes the simulated noisy InSAR tensor with 5 dB Gaussian noise (left) and 10 dB Gaussian noise (right) with different parameters settings.

Eq. (13) is transformed into its augmented Lagrangian function, which can be solved by alternating direction multiplier method (ADMM) [31] to obtain the low rank tensor. The weights can be updated by (14)

$$
\begin{aligned}
w_{nj} &= \frac{1}{\sigma_j(\mathbf{T}_{(n)}) + \varepsilon_1} \\
\mathcal{W}_{\mathcal{E}} &= \frac{1}{|\mathcal{E}| + \varepsilon_2}
\end{aligned}
\tag{14}
$$

where ε_1 and ε_2 are predetermined positive constants and set to prevent denominator from zero.

However, as the initialization step, the setting of these two predetermined parameters limits the accuracy of WHoRPCA. A simulated InSAR tensor in TG1 is selected as experimental data to analyze the influence of the initialization parameters. The outlier ratio is set to be 30%. Gaussian noise is added to this simulated InSAR tensor with SNR of 5dB and 10dB, respectively.

The Mean Square Error (MSE) is calculated between the recovered InSAR tensor and the clean one to evaluate the filter performance, i.e. MSE(angle($\mathcal{T}_0 \odot$ conj($\mathcal{L}$))), where $\mathcal{T}_0$ is the clean complex InSAR stack data, $\mathcal{L}$ is the filtered result of the noisy complex InSAR tensor $\mathcal{T}$. conj($\cdot$) is complex conjugate operator. MSE mentioned in later obeys this calculation method.

The result is shown in Fig. 3 with respect to different pairs of ε_1 and ε_2. Considering that the appropriate parameters depend on SNR and other variables, when the improper parameters are selected, it produces the unsatisfactory results that deteriorate MSE. Therefore, the setting of these two parameters is challenging for the application of WHoRPCA, leading to the worse robustness than HoRPCA.

By introducing the weight strategy into HoRPCA, the flexibility of tensor decomposition has been improved, and its performance has been verified by simulated and real data in related research [17]. As shown in Fig. 2, the Tucker rank of low rank tensor obtained by WHoRPCA is higher than that of HoRPCA, which indicates that WHoRPCA has a better ability to estimate the low rank tensor. Although excessively smoothing caused by HoRPCA has been modified by WHoRPCA, more predetermined parameters are
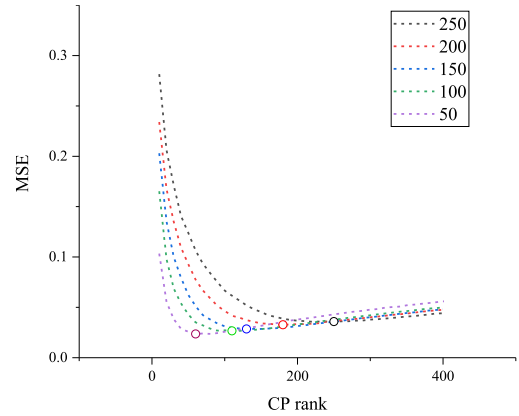

FIGURE 4. MSE between the clean reference and filtered InSAR tensor acquired by CP decomposition, when the different CP ranks are predetermined. The most suitable CP rank of InSAR tensor is influenced by different spatial baseline ranges, represented by the dotted lines with different colors.

introduced into the algorithm, and it is difficult to set the suitable parameters when the condition of noise varies.

IV. ANALYSIS OF InSAR TENSOR FILTER ON CP RANK
In CP decomposition, InSAR tensor $\mathcal{T} \in \mathbb{C}^{I_1 \times I_2 \times I_3}$ can be decomposed to the sum of outer products of vectors shown as (15).

$$
\mathcal{T} = \sum_{p=1}^{R} (\xi_p a_p^{(1)} \circ a_p^{(2)} \circ a_p^{(3)})
\tag{15}
$$

where $a_p^{(1)}$, $a_p^{(2)}$ and $a_p^{(3)}$ are three orthogonal vectors, called as Kronecker basis, $\xi_p \in \mathbb{R}$ is a coefficient of the pth Kronecker basis, and R represents CP rank, corresponded to the high order extension of the matrix rank.

CP rank should be predetermined before CP decomposition, which is challenging for the computation of appropriate CP rank [27], and its convex relaxation is intractable. The common strategy is to iterate CP rank from 1 until a better result is achieved. To assess the performance of CP rank used as InSAR tensor rank, a set of InSAR tensors in TG3 has been selected as experimental data. As shown in Fig. 4, the MSE is calculated when CP rank is predetermined to different values.

According to Fig. 4, the noisy InSAR tensor is well recovered by CP decomposition with an appropriate CP rank. For example, when the value of CP rank is 250, the MSE of the filtered tensor with the spatial baseline range of 250 m is around 0.90, which is more accurate to the same noisy tensor filtered by HoRPCA. On the contrary, some noise will be remained in the filtered interferogram with higher CP rank, or over smoothing will occur in the case of lower CP rank. Obviously, MSE is a good indicator of selecting CP rank, however, there is no clean (or ideal) reference in reality, so it is difficult to set a suitable CP rank before CP decomposition. When choosing the appropriate CP rank according to the number of residuals remaining in the filtered
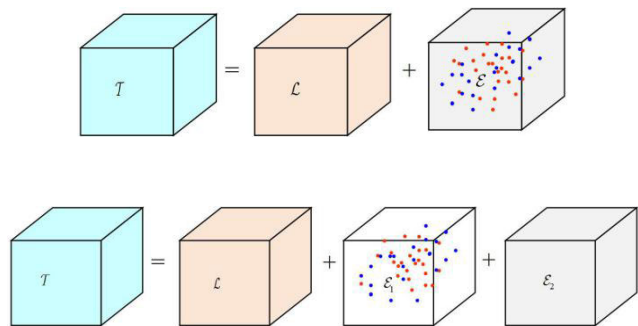
FIGURE 5. The simplified InSAR phase tensor model (above) and its improved form (below).
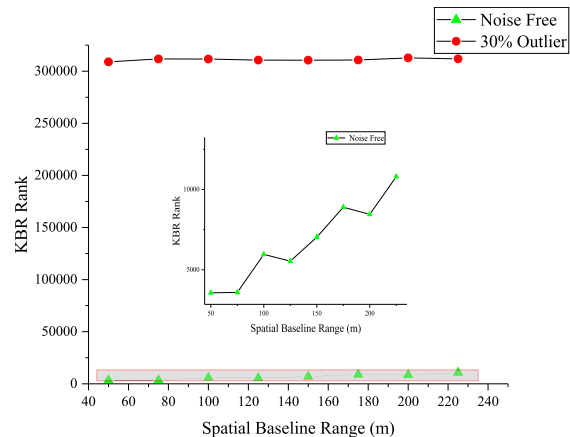

FIGURE 6. KBR of simulated tensor group (TG) 1 and 3. TG1 is a collection of noise-free simulated tensors with different baseline ranges. Spatial baseline range equals x m, denoted as the baseline for one interferogram in InSAR tensor randomly distributed in [−x, x] m. TG3 is TG1 added 5 dB Gaussian noise and 30% outlier.

interferogram, the reduction of residuals may be caused by excessive smoothing.

In summary, CP decomposition is based on the definition of tensor rank considering the entire tensor rather than each mode of tensor. Although InSAR tensor recovery with CP rank is still challenging, this definition of tensor rank offers a good idea to measure the sparsity of InSAR tensor.

V. InSAR TENSOR FILTER METHOD BASED ON KBR

A. IMPROVED InSAR TENSOR MODEL

According to the Persistent Scatters InSAR (PSI) model [28], [29], the decorrelation noise is additive in interferometric phase, and it contains both isolated phase jump-points caused by spatial under-sampling and the Gaussian noise, i.e. system thermal noise, dispersed throughout the interferogram. However, the previous InSAR tensor model assumes that the Gaussian noise and the isolated phase jump-points will be extracted as an entire outlier tensor (shown in Eq. (5)).

It is noted that these two types of noise have different distribution properties. The phase jump-points uniformly distribute in the interferogram, while the Gaussian noise satisfies the normal distribution, which is caused by system noise and several decoherent factors. Therefore, the observed InSAR tensor consists of low rank tensor, phase jump-points tensor and Gaussian noise tensor, which is shown in (16).

$$\mathcal{T} = \mathcal{L} + \mathcal{E}_1 + \mathcal{E}_2 \tag{16}$$

where $\mathcal{E}_1$ is the phase jump-points (sparse noise) tensor and $\mathcal{E}_2$ is the Gaussian noise tensor. The comparison between two models is more intuitively shown in Fig. 5.

B. KBR

As explained above, Tucker rank concerns the modes of the tensor while CP rank considers the entire tensor, and both definitions have limitations when they are applied to measure the sparsity of InSAR tensor. As a result, KBR, as a recently proposed definition of tensor rank, combines the advantages of Tucker rank and CP rank by concerning the entire tensor and its each mode. The KBR of a third-order tensor $\mathcal{T}$ can be

calculated by (17).

$$f(\mathcal{T}) = t \, \|\mathcal{S}\|_0 + (1 - t) \prod_{n=1}^{3} rank(\mathbf{T}_{(n)}) \tag{17}$$

where $\mathcal{S}$ is the core tensor of $\mathcal{T}$ calculated by HoSVD, t is a predetermined coefficient between (0, 1).

The first term of (17) is required to be solved in sparse non-negative tucker decomposition [34], while InSAR tensor in complex domain is obviously a more complicated data. The relaxation of KBR to simplify the computation is shown in (18).

$$f^*(\mathcal{T}) = t \sum_i (\log(|s_i| + \delta) - \log(\delta))/(-\log(\delta))$$

$$+ (1 - t) \prod_{n=1}^{3} \left(\sum_m \log(\sigma_m(\mathbf{T}_{(n)}))/(-\log(\delta)) \right) \tag{18}$$

where δ is a small positive number, $|s_i|$ is ith nonzero element of $\mathcal{S}$.

The sparsity of the real part of complex InSAR tensors in TG1 and TG3 are calculated by (18) and shown in Fig. 6. In this figure, the KBR rank of the noisy InSAR tensor is larger than the corresponding clean one. Consequently, it is feasible to introduce KBR to construct low rank decomposition and realize the InSAR tensor filtering. The complex InSAR tensor can be addressed to real-valued pairs, e.g. phase/amplitude or real/imaginary parts of tensor. However, considering the 2π-wrapping of interferometric phase, KBR is applied to measure the rank of real/imaginary parts of complex phase tensor separately in our work.

C. InSAR TENSOR DECOMPOSITION METHOD BASED ON KBR

In this section, the proposed filter of multi-baseline and multi-temporal InSAR stack data is demonstrated in details. We first split the InSAR stack data into real and imaginary

tensors, and the optimization algorithm of KBR-RPCA [35] is utilized to decompose the real tensor and imaginary tensor, respectively. The constraint is imported to the decomposition because of the elimination of amplitude information, shown in (19). Therefore, based on the principle of KBR, the novel phase filtering method, named as KBR-InSAR, is proposed as follows:

$$\{\mathcal{L}, \mathcal{E}_1, \mathcal{E}_2\} = KBRRPCA(\mathcal{T}_{real}) + j * KBRRPCA(\mathcal{T}_{imag})$$
$$s.t. \ \mathcal{T}_{real} \odot \mathcal{T}_{real} + \mathcal{T}_{imag} \odot \mathcal{T}_{imag} = \mathcal{O} \quad (19)$$

where $\mathcal{O}$ is an all-1 tensor. $\mathcal{T}_{real}$ is the real part of InSAR tensor $\mathcal{T}$, and $\mathcal{T}_{imag}$ is the imaginary part. $KBRRPCA(\cdot)$ represents the algorithm of KBR-RPCA [35].

The decomposition of complex InSAR tensor is supported by the improved InSAR phase tensor model. Taking the solution of real part as an example, and shown in the followings:

$$KBRRPCA(\mathcal{T}_{real})$$
$$= \min_{\mathcal{I}_{real}, \mathcal{N}_1, \mathcal{N}_2} f^*(\mathcal{I}_{real}) + \alpha \|\mathcal{N}_1\|_1 + \frac{\beta}{2} \|\mathcal{N}_2\|_F^2$$
$$s.t. \ \mathcal{T}_{real} = \mathcal{I}_{real} + \mathcal{N}_1 + \mathcal{N}_2 \quad (20)$$

where $\mathcal{I}_{real}$ is the real part of information tensor $\mathcal{L}$, $\mathcal{N}_1$ is composed of isolated phase jump-points in $\mathcal{T}_{real}$, and $\mathcal{N}_2$ represents Gaussian noise in $\mathcal{T}_{real}$.

We first convert the (20) to its augmented Lagrangian function as follows:

$$KBRRPCA(\mathcal{T}_{real}) = \underset{\mathcal{L}, \mathcal{E}, \mathcal{N}}{\arg\min} f^*(\mathcal{I}_{real}) + \alpha \|\mathcal{N}_1\|_1$$
$$+ \frac{\beta}{2} \|\mathcal{I}_{real} + \mathcal{N}_1 - \mathcal{T}_{real}\|_F^2$$
$$+ \sum_{n=1}^{3} \langle \mathcal{I}_{real} - \mathcal{M}_n, \mathcal{P}_n \rangle$$
$$+ \sum_{n=1}^{3} \frac{\sigma}{2} \|\mathcal{I}_{real} - \mathcal{M}_n\|_F^2$$
$$(\mathcal{I}_{real} = \mathcal{S}_r \times_1 \mathbf{U}_{r(1)} \times_2 \mathbf{U}_{r(2)} \times_3 \mathbf{U}_{r(3)}) \quad (21)$$

where $\mathcal{S}_r$ is the core tensor of $\mathcal{I}_{real}$, and $\mathbf{U}_{r(n)}$ is a mode-n matrix of $\mathcal{I}_{real}$. $\mathcal{M}_n$ is an auxiliary tensor initialized as $\mathcal{T}_{real}$ and updating with iterations. $\mathcal{P}_n$ is the Lagrange multiplier, and σ is a regularization coefficient.

Then the low rank tensor $\mathcal{I}_{real}$ is acquired as the filtered result by using ADMM algorithm to solve the augmented Lagrangian function in (21). The imaginary part of InSAR tensor uses the similar optimization method as the above-mentioned process. Finally, the error tensor $\mathcal{R}$ of filtered tensor is calculated by

$$\mathcal{R} = \frac{\mathcal{O}}{\mathcal{I}_{real} \odot \mathcal{I}_{real} + \mathcal{I}_{imag} \odot \mathcal{I}_{imag}} \quad (22)$$

where $\mathcal{I}_{imag}$ is the low rank tensor of $\mathcal{T}_{imag}$, and $\mathcal{L} = \mathcal{I}_{real} + j \cdot \mathcal{I}_{imag}$. The average value of all elements in $\mathcal{R}$ is compared to a threshold to judge whether the normalized
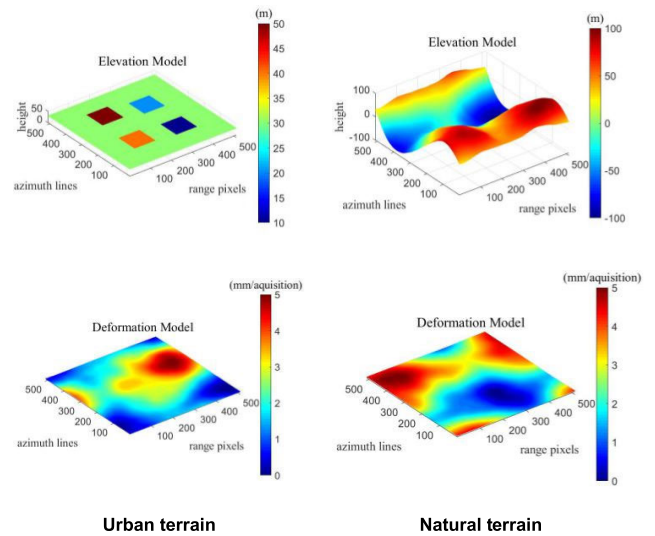

FIGURE 7. The terrain models and deformation models of two simulated InSAR tensors. A simulated continuous undulating topography is used to represent natural terrain, and a flat terrain with several raised regular squares represents the case of urban with buildings.
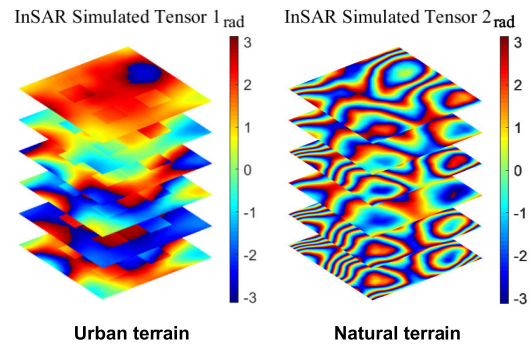

FIGURE 8. Two simulated InSAR phase tensors (partial display).

InSAR tensor has been obtained through the current iteration. If not, the optimization is repeated until the convergence condition is satisfied. In summary, KBR-InSAR is presented as Algorithm 1.

The optimization process of KBR-InSAR is mainly consumed in KBR-RPCA algorithm and the update of error tensor, the real and imaginary parts of InSAR tensor $\mathcal{T}$. In fact, updating $\mathcal{M}_n$ and $\mathbf{U}_{r(n)}$ is the main per-iteration cost of KBR-RPCA, it needs to compute SVDs of $I_n \times (\prod_{m \neq n} I_m)$ ($m = 1, 2, 3$) matrix and $I_n \times I_n$ matrix respectively, and the time cost of a SVD of $n \times n$ matrix is $O(n^3)$. The process of KBR-RPCA is terminated until the current deviation of the low-rank tensor between iterations is smaller than a preset threshold θ. Considering a third-order tensor, i.e. $\mathcal{T} \in \mathbb{C}^{I_1 \times I_2 \times I_3}$, is used as input for KBR-InSAR and supposing the number of iterations is M, therefore, the time complexity of the proposed algorithm is $O(M \times (\log \theta \times (I_1^3 + I_2^3 + I_3^3) + I_1 \times I_2 \times I_3))$, and its space complexity is $O(I_1 \times I_2 \times I_3)$.
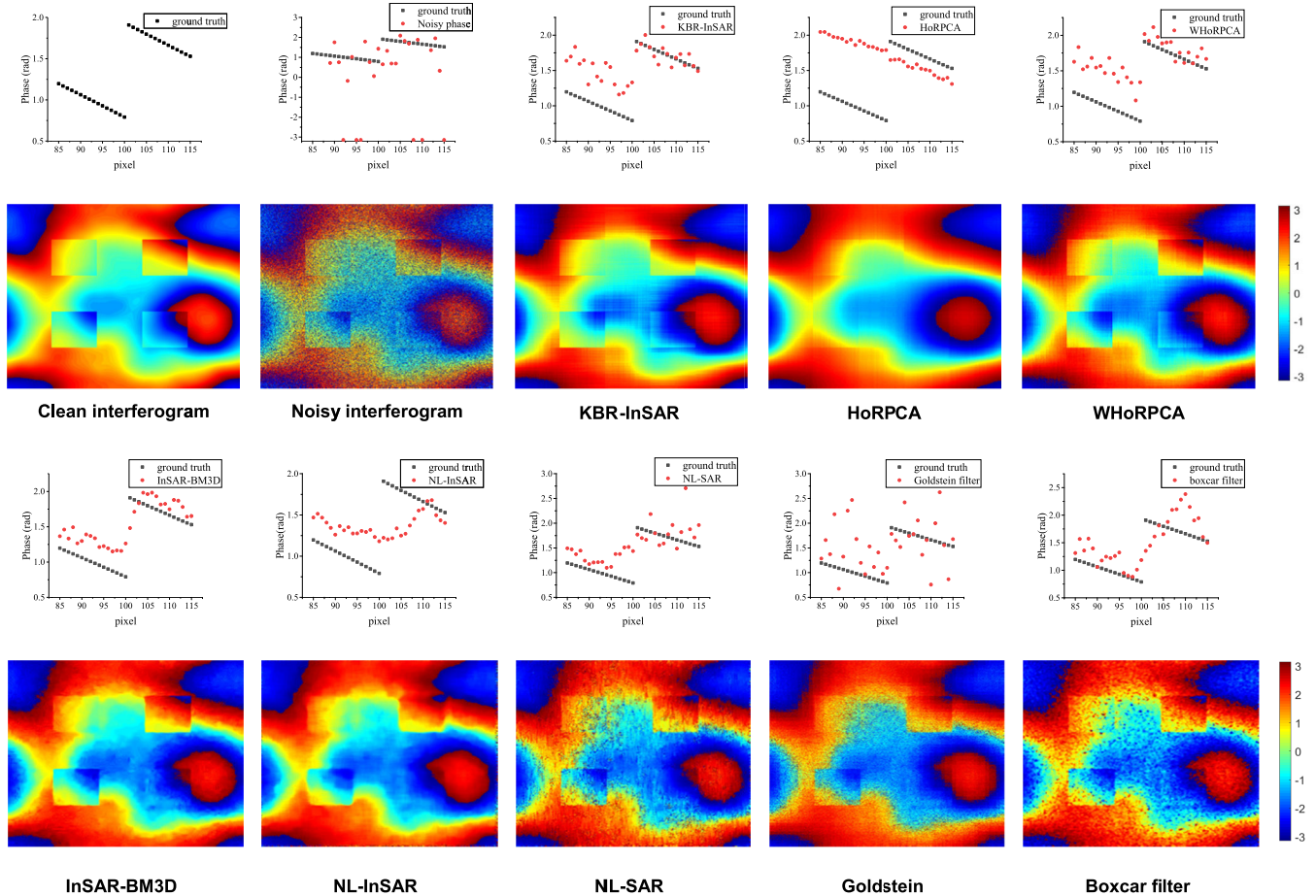
FIGURE 9. The filtered results and their phase profiles crossing a raised square. The clean interferogram and its noisy version are shown in the upper left. The pixels value (phase) in a local position of the filtered interferogram and its visual observation, which is selected from InSAR stack data 2, is used to evaluate these filters, i.e., KBR-InSAR, HoRPCA, WHoRPCA, InSAR-BM3D, NL-InSAR, NL-SAR, Goldstein and Boxcar filter. Filters based on non-local, i.e. InSAR-BM3D, NL-InSAR and NL-SAR, obtain the continuous phase values smoothly, which are not suitable for filtering the region with phase changed rapidly.

Algorithm 1 Algorithm for KBR-InSAR

Input: InSAR Phase Tensor: $\mathcal{T}$

1: **initialize:** Set **threshold** $= 1.001$
2: $\mathcal{T} = \mathcal{T}_{real} + j * \mathcal{T}_{imag}$
3: **while** mean$(\mathcal{R}) >$ **threshold do**
4:     Normalization $\mathcal{T}_{real}, \mathcal{T}_{imag}$
5:     $\mathcal{I}_{real} = KBRRPCA(\mathcal{T}_{real})$
6:     $\mathcal{I}_{imag} = KBRRPCA(\mathcal{T}_{imag})$
7:     Denormalization $\mathcal{I}_{real}, \mathcal{I}_{imag}$
8:     Update $\mathcal{R}$ by (22)
9:     Update $\mathcal{T}_{real}$ by $\mathcal{T}_{real} = I_{real} \odot \sqrt{\mathcal{R}}$
10:     Update $\mathcal{T}_{imag}$ by $\mathcal{T}_{imag} = I_{imag} \odot \sqrt{\mathcal{R}}$
11: **end while**
12: $\mathcal{T} - \mathcal{T}_{real} + \mathcal{T}_{imag} * j$

Output: phase $=$ angle$(\mathcal{T})$

VI. RESULTS AND ANALYSIS

In this section, we present and analyze the quantitative and qualitative results to prove the effectiveness of KBR-InSAR.

Experiments are performed on both simulated and real InSAR stack data.

A. SIMULATED DATA

The first experiment is to compare the performance of tensor-based filters (i.e. HoRPCA, WHoRPCA and KBR-InSAR). The parameters of HoRPCA are set as the authors did in their published papers. It is noted that the result of WHoRPCA is greatly influenced by the initialization parameters. Therefore, we select the best filtered results obtained during the process of traversal parameters.

A complex InSAR tensor is generated as experimental data with 25 interferograms, and each interferogram has 512×512 pixels. The range of spatial baseline is 250m, which means the baselines of interferograms in the simulated tensor are randomly distributed from-250m to 250m. To sufficiently analyze the performance of these tensor-based filters, the circular complex standard Gaussian noise with SNR of 5dB, 7dB and 3dB are imported to the simulated InSAR stack data, and partial pixels in each interferogram
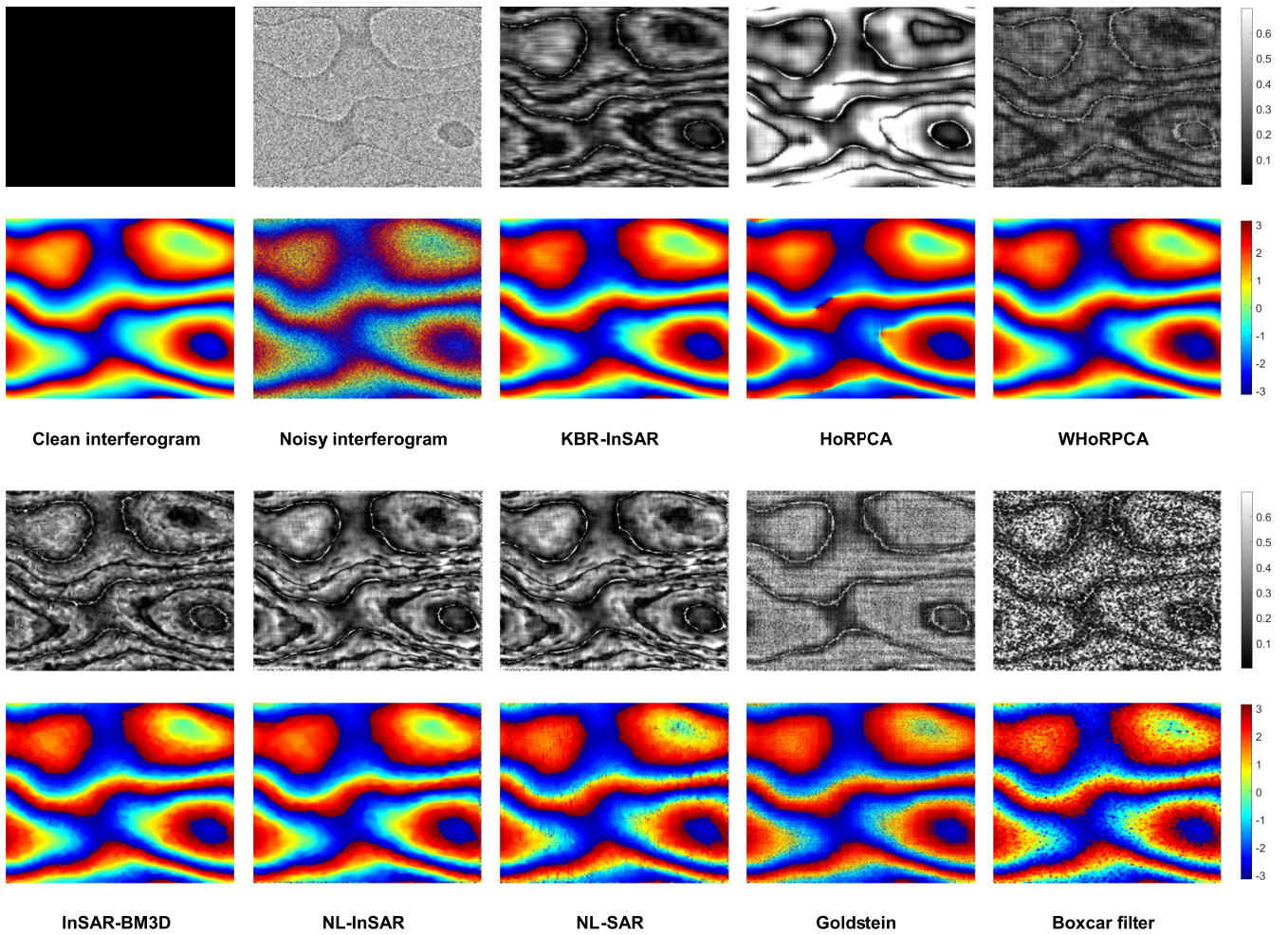
FIGURE 10. Filtered images (Bottom) and their error images (Top) generated by KBR-InSAR and other reference filters for the sparse fringes interferogram in the simulated InSAR phase tensor with a natural terrain.

TABLE 1. Results on different tensor depth.

Noise Intensity	Outlier Ratio	Tensor Depth	HoRPCA	WHoRPCA	KBR-InSAR
7dB	30%	25	3.52	0.94	0.72
7dB	30%	20	4.14	0.98	0.74
7dB	30%	10	5.59	1.095	0.87

TABLE 2. Results on different outlier ratio.

Noise Intensity	Outlier Ratio	Tensor Depth	HoRPCA	WHoRPCA	KBR-InSAR
7dB	10%	25	1.34	0.54	0.47
7dB	20%	25	2.20	0.70	0.56
7dB	30%	25	3.52	0.94	0.72
7dB	40%	25	6.21	1.30	1.14

TABLE 3. Results on different noise intensity.

Noise Intensity	Outlier Ratio	Tensor Depth	HoRPCA	WHoRPCA	KBR-InSAR
7dB	10%	25	1.34	0.54	0.47
5dB	10%	25	1.69	0.69	0.57
3dB	10%	25	2.25	0.87	0.71

of InSAR stack data are randomly replaced by $-\pi$ or π according to the outlier ratio.

MSE is an effective evaluation applied to measure the filtered results, and the evaluation results of MSE are shown in Table 1 to 3. Especially, Table 1 proves that KBR-InSAR maintains the accuracy when the tensor depth is relatively small, where tensor depth is the number of interferograms contained in the InSAR stack data. Based on the improved InSAR phase tensor model, the noise in InSAR stack data is further distinguished by KBR-InSAR. KBR-InSAR is superior to other tensor-based methods whether in the case of strong Gaussian noise (see Table 3) or high outlier ratio

(see Table 2). Since most of the obtained interferograms have serious noise, it is proved that KBR is the best low-rank approximation method for the InSAR tensor.

The second experiment aims to further compare the results of proposed KBR-InSAR and other widespread filters
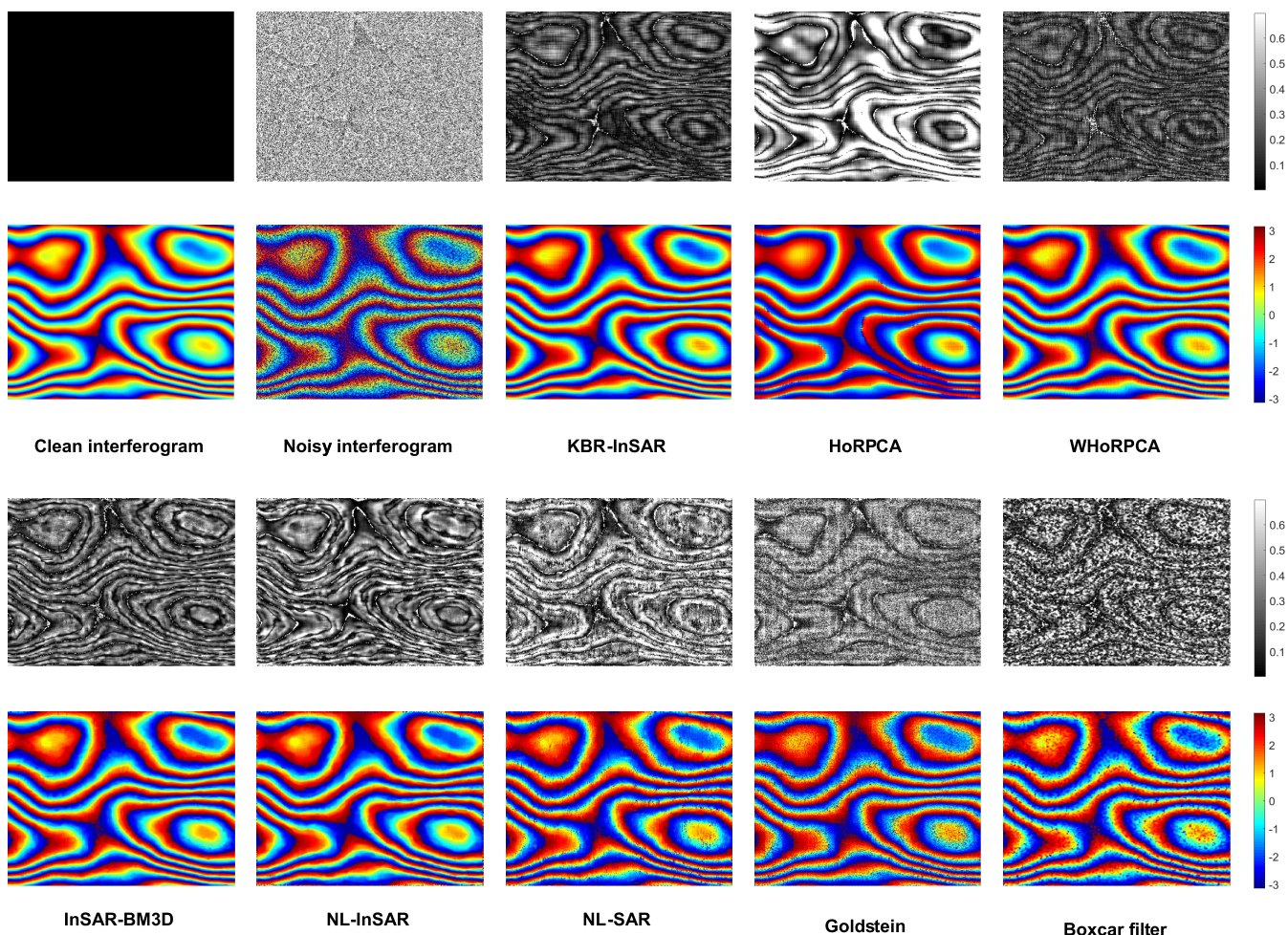
FIGURE 11. Filtered images (Bottom) and their error images (Top) generated by KBR-InSAR and other reference filters for the dense fringes interferogram in the simulated InSAR phase tensor with a natural terrain.

operating on a single interferometric pair in a certain noisy condition. Two sets of InSAR stack data, containing 25 interferograms with 512×512 pixels for each, are generated: One is a flat terrain with four squares raised as appeared in urban area, and the other is a continuous natural topography as shown in Fig. 7. The circular complex standard Gaussian noise with SNR of 5dB is added to these simulated InSAR stack data. 30% pixels in each interferogram are randomly selected and replaced by $-\pi$ or π. The simulated InSAR tensor is partially shown in Fig. 8.

The comparative methods include five traditional filtering methods, i.e. boxcar filter with the window of 5×5, Goldstein filter where the patch is 32×32 and α is 0.5, NL-SAR with a 21×21 search window and its patch is set from 3 to 11, NL-InSAR where the search window is 21×21 and the patch is 7×7, and InSAR-BM3D, its parameters are the same as the published study [15].

The average of MSEs calculated by all interferograms in InSAR stack data objectively evaluates the performance of these filtering methods, as shown in Table 4. Furthermore, the number of residues remaining in the filtered

interferograms is also used as an effective evaluation, as shown in Table 5. The MSE in Table 4 is lower than that in Table 1, 2 and 3, that is because the range of spatial baseline used in second simulation experiment is decreasing, and dense fringes rarely appear. KBR-InSAR outperforms other filtering methods for processing two simulated InSAR stack data in terms of the MSE result. According to the residues in Table 5. HoRPCA filter provides the best result sometimes because of over smoothing. Further verification is shown in Fig. 9, and most details are lost in the filtered result of HoRPCA.

Fig. 9 shows the global filtered results of eight different filters for a selected interferogram, and the phase profiles with a length of 30 pixels crossing the edge of a raised square in this interferogram. The first and third rows of Fig. 9 are phase profiles crossing the edge, and the black square represents the noise-free phase and the red circle represents the filtered phase. It can be seen the boxcar filter generates a low-resolution filtered result with losing many details in fringes. The Goldstein filter provides an unsatisfactory performance of noise suppression because of low SNR in our simulated
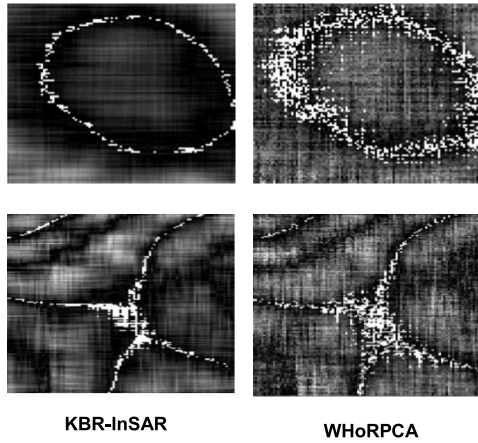
FIGURE 12. The partial enlarged detail of the error images with KBR-InSAR (left column) and WHoRPCA (right column). The error images at top are [320:420, 300:400] of the simulated interferogram shown in Fig.10, and the error images at bottom are [250:400, 150:250] of the simulated interferogram shown in Fig.11.
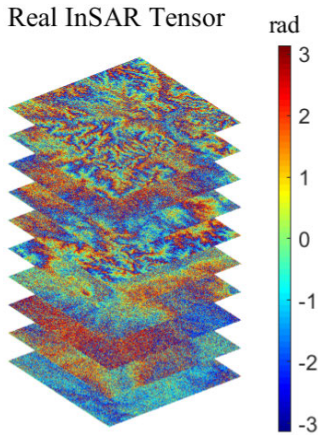

FIGURE 13. The real InSAR phase tensor collected from Sentinel-1B (partial display).

TABLE 4. MSE for proposed method and referenced methods.

Method	MSE of InSAR stack data 1	MSE of InSAR stack data 2
KBR-InSAR	0.29	0.46
WHoRPCA	0.64	0.79
HoRPCA	0.89	1.12
InSAR-BM3D	0.43	0.53
NL-SAR	0.66	1.22
NL-InSAR	0.37	0.79
GoldStein	1.05	1.56
Boxcar	0.80	1.02

data. It can be noticed that the methods based on nonlocal (i.e. NL-InSAR, NL-SAR and InSAR-BM3D) present an obvious error in the region of phase fast-changing, e.g. some edges of the raised squares. Weighted averaging of the similar patches or blocks, as an important step in these algorithms, results in phase mutation, and the topographic details is reduced.

TABLE 5. Residues for proposed method and referenced methods.

Method	Residues (14th)	Residues (17th)	Residues (8th)
KBR-InSAR	4730	597	865
WHoRPCA	13535	7141	13392
HoRPCA	4942	950	146
InSAR-BM3D	5055	2129	1278
NL-SAR	53757	5912	14674
NL-InSAR	8235	1967	3666
GoldStein	95704	15654	64032
Boxcar	31299	4907	23436

TABLE 6. Evaluation of filtering results of the simulated InSAR tensor with the complicated building.

	Method	MSE
Tensor-based Filters	KBR-InSAR	0.3670
	WHoRPCA	0.8891
	HoRPCA	0.9431
Adaptive Filters	NL-SAR	0.5807
	Goldstein	1.1214
	Lee	1.8843

The filter of HoRPCA has a good restoration in most of the interferograms, but its performance deteriorates at the edges of the raised squares, due to the over-smoothing caused by the lower Tucker rank during the tensor decomposition. On the contrary, KBR-InSAR provides a better performance of removing noise meanwhile preserving the original fringes.

Fig. 10 and Fig. 11 present a filtered interferogram in simulated InSAR stack data with natural terrain and its error image (i.e. the difference between the filtered result and the ground truth). The more correct pixels (black color) in these figures, the better filtering results are obtained. Therefore, according to the error images of different filtering methods, KBR-InSAR obviously outperforms other filters whether the fringes are dense or sparse.

The local comparison between WHoRPCA and KBR-InSAR is shown in Fig. 12. The error images at top is [320:420, 300:400] of the simulated interferogram shown in Fig. 10, and the error images at bottom is [250:400, 150:250] of the simulated interferogram shown in Fig. 11. The error pixels (white color) of KBR-InSAR are smaller in number and more concentrative in distribution, which indicates the KBR-InSAR performs better in fringe preservation, especially at the position of 2π jump.

B. REAL DATA

The experiment on ten SAR complex images acquired by Stentinel-1B from July to November 2018, covering Changbai Mountain area in Northeast China, has been carried out. The master acquisition (August 17, 2018) is selected for the coregistration with all slave images. A complex InSAR tensor is formed by these coregistered SLC images, as shown in Fig. 13. The filtering for this InSAR stack data is relatively challenging because of the low SNR in this real data.
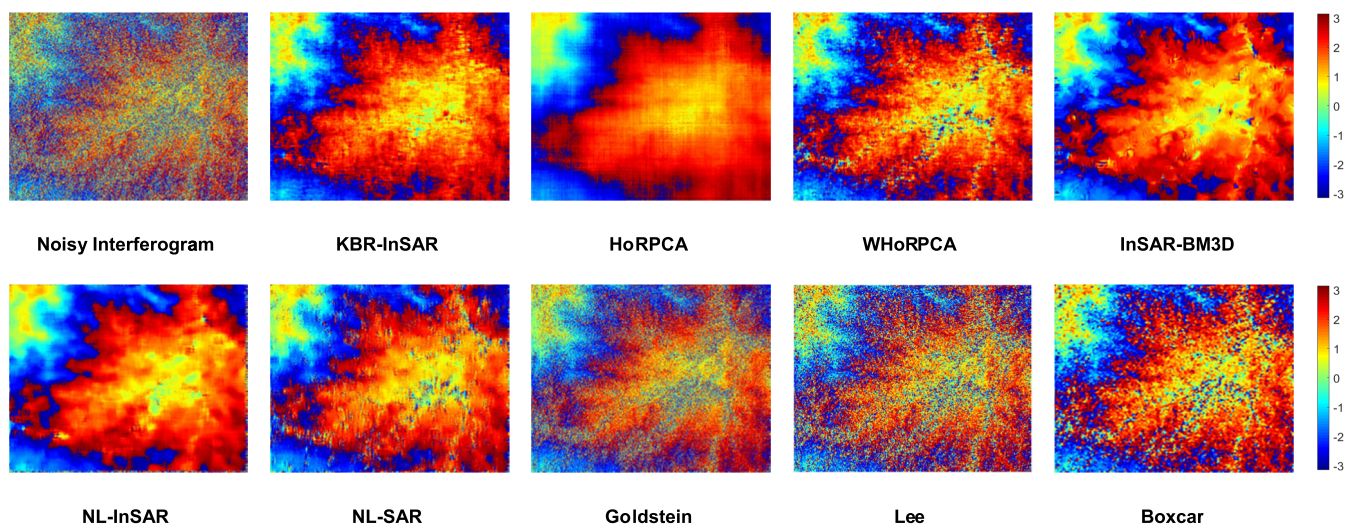
FIGURE 14. The filtered results acquired by KBR-InSAR and other widespread filters when the fringes are sparse in the selected interferogram of the real InSAR tensor collected from Sentinel-1B. The filtering result of HoRPCA is too smooth to maintain details, and the results acquired by WHoRPCA, NL-SAR, Goldstein, Lee and Boxcar are still noisy. The straight stripes caused by the limitation of InSAR-BM3D are obvious. KBR-InSAR has a satisfactory filtering result.
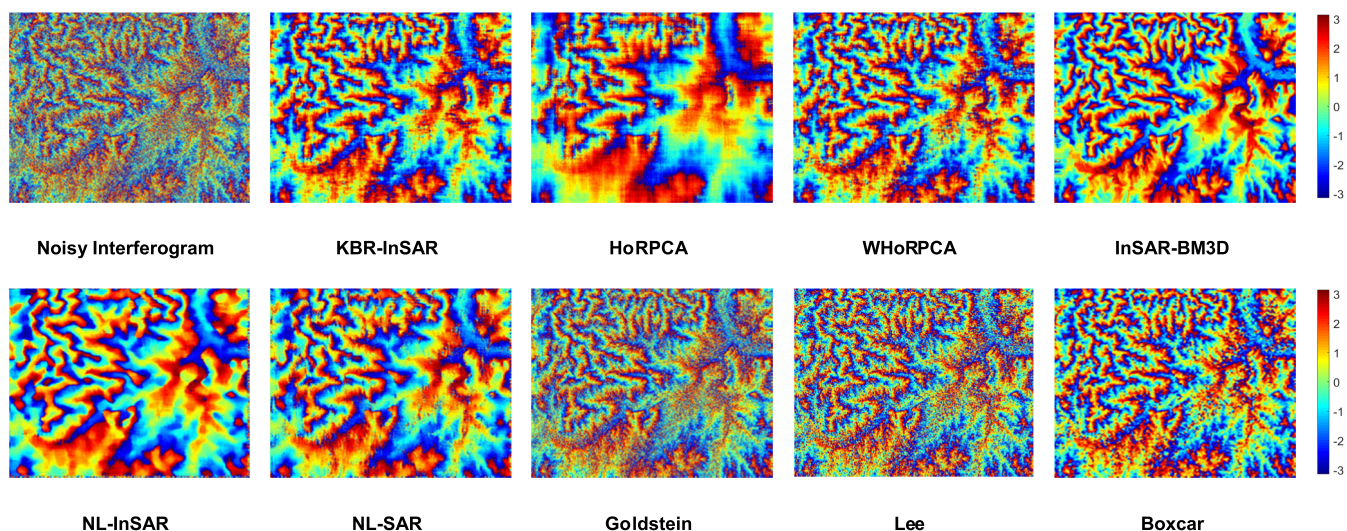

FIGURE 15. The filtered results acquired by KBR-InSAR and other widespread filters when the fringes are dense in the selected interferogram of the real InSAR tensor collected from Sentinel-1B. The results acquired by HoRPCA, NL-SAR and NL-InSAR are over smooth and lose most details. The results filtered by InSAR-BM3D are attractive, but hardly correct in dense fringes (see the details in Figure 19).

Fig. 14 presents the filtered results under the condition of sparse fringes, and the dense fringes case is shown in Fig. 15. The filtered interferograms acquired by boxcar and Goldstein remain more noise than other filters obviously. Although HoRPCA almost clears all the residues, the ability of fringes preservation is insufficient. The result of HoRPCA may be more appealing than WHoRPCA, but it is hard to guarantee that is an accurate filtered result, which is more intuitive in the condition of dense fringes. WHoRPCA preserves the details of fringes by introducing weights into HoRPCA algorithm, however, it smooths the product of weight tensor and low rank tensor rather than only low-rank tensor, and thus causes the slight remaining noise in the filtered result. NL-SAR
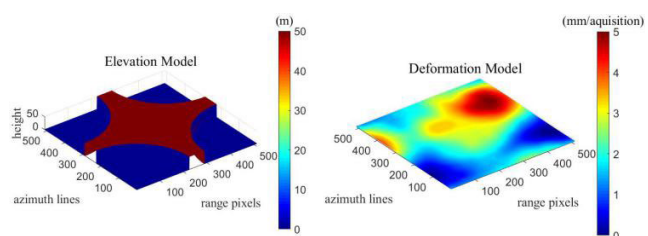

FIGURE 16. The terrain model and deformation model of the simulated InSAR tensor with a complicated building.

and NL-InSAR excessively smooth the interferometric phase and sacrifice many details, which is more obvious when the fringes are dense. Obviously, averaging the similar patches
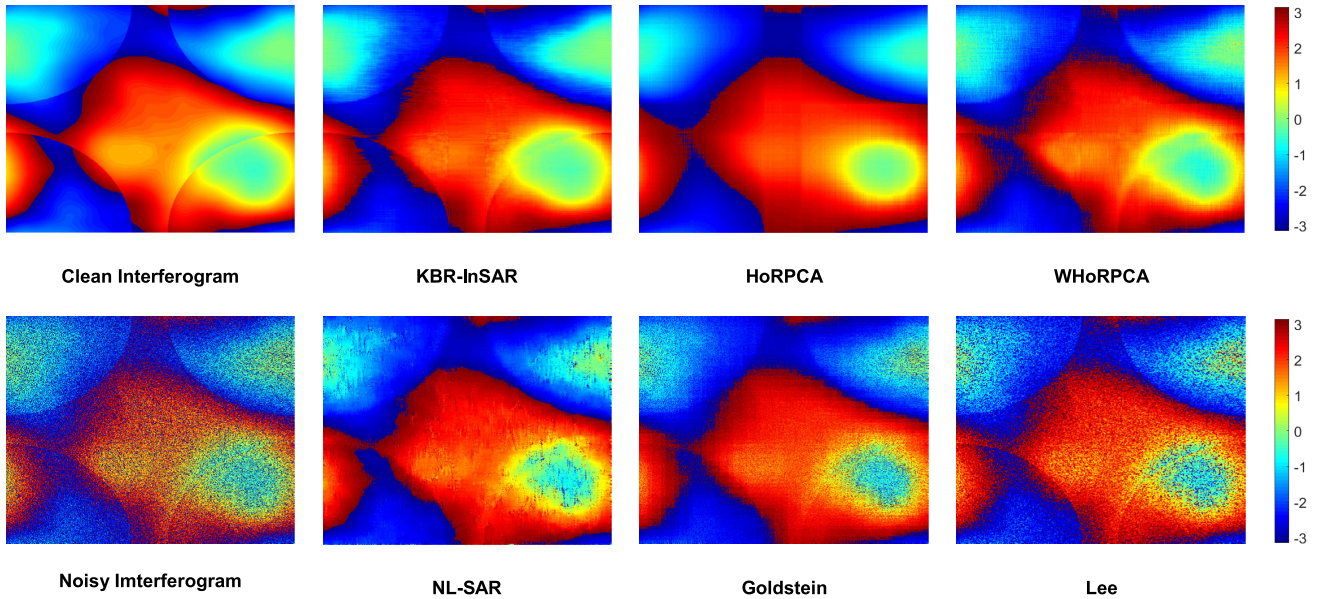
FIGURE 17. One interferogram in the simulated InSAR tensor with the complicated building and its filtered results acquired by tensor-based filters and adaptive filters.
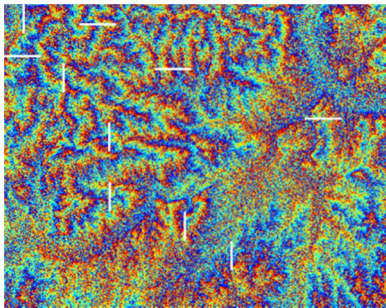

FIGURE 18. A noisy interferogram in real InSAR phase tensor collected from Sentinel-1B shown in Figure 15. The short white lines on the interferogram are used to illustrate the phase profiles shown in Figure 19.

is an unsuitable strategy for filtering phase changed rapidly, after all, this phase mutation reflects the details of the terrain, not caused by noise. The same conclusion can be found in Fig. 9 and its related explanations.

VII. DISCUSSIONS

A. PERFORMANCE IN SIMULATED DATA

To further prove the reliability of KBR-InSAR, then a simulation experiment is supplied in this section. The elevation model of the simulated InSAR tensor is a vertical structure with curvy edges as shown in Fig. 16. The circular complex standard Gaussian noise with SNR of 5dB is added to these simulated InSAR stack data. 30% pixels in each interferogram are randomly replaced by $-\pi$ or π. One of interferograms in this InSAR tensor is selected to directly compare the filtered results acquired by tensor-based methods and adaptive methods, as shown in Fig. 17. The phase boundary caused by curvy edges in elevation model is clear

in KBR-InSAR, however, the filtered results in HoRPCA and WHoRPCA are ambiguous, not to mention those adaptive methods. Therefore, it indicates that KBR-InSAR superior to other tensor-based methods. On the view of quantitative evaluation, KBR-InSAR is also superior to adaptive filters as shown in Table 6.

Then to evaluate the computation overhead and time consumption of the tensor-based filters. In this experiment, CPU is Intel (R) Xeon (R) CPU E5-2620 v4 with the frequency of 2.10 GHZ. Three tensor-based methods are very close in spatial complexity, and KBR-InSAR has the minimum consumption about 0.45 GB memory. In time consumption, the average iteration time of WHoRPCA is 6.873s when the size of simulated data is $512 \times 512 \times 25$, and HoRPCA is about 11.855s, and KBR-InSAR is about 0.819s. In total time-consumption, WHoRPCA is 0.06h with 30 iterations, and HoRPCA has 0.171h with 52 iterations. Although KBR-InSAR has a greater consumption, i.e. 0.357h caused by 1571 iterations, it is a time-accuracy balance choice. Predictably, the time-consumption of KBR-InSAR can be significantly decreased by using parallel computation.

B. PERFORMANCE IN REAL DATA

In the experiment of real InSAR stack data, some phase profiles, marked as the white short lines in Fig. 18, in different filtered results are depicted to prove the superiority of our method, as shown in Fig. 19. KBR-InSAR has stability to obtain satisfactory filtered result with low SNR whether at sparse or dense fringes. On the contrary, there are some phase steps appearing in the phase profiles of InSAR-BM3D, which are unacceptable in application. It is noted that all tensor-based methods have a good property
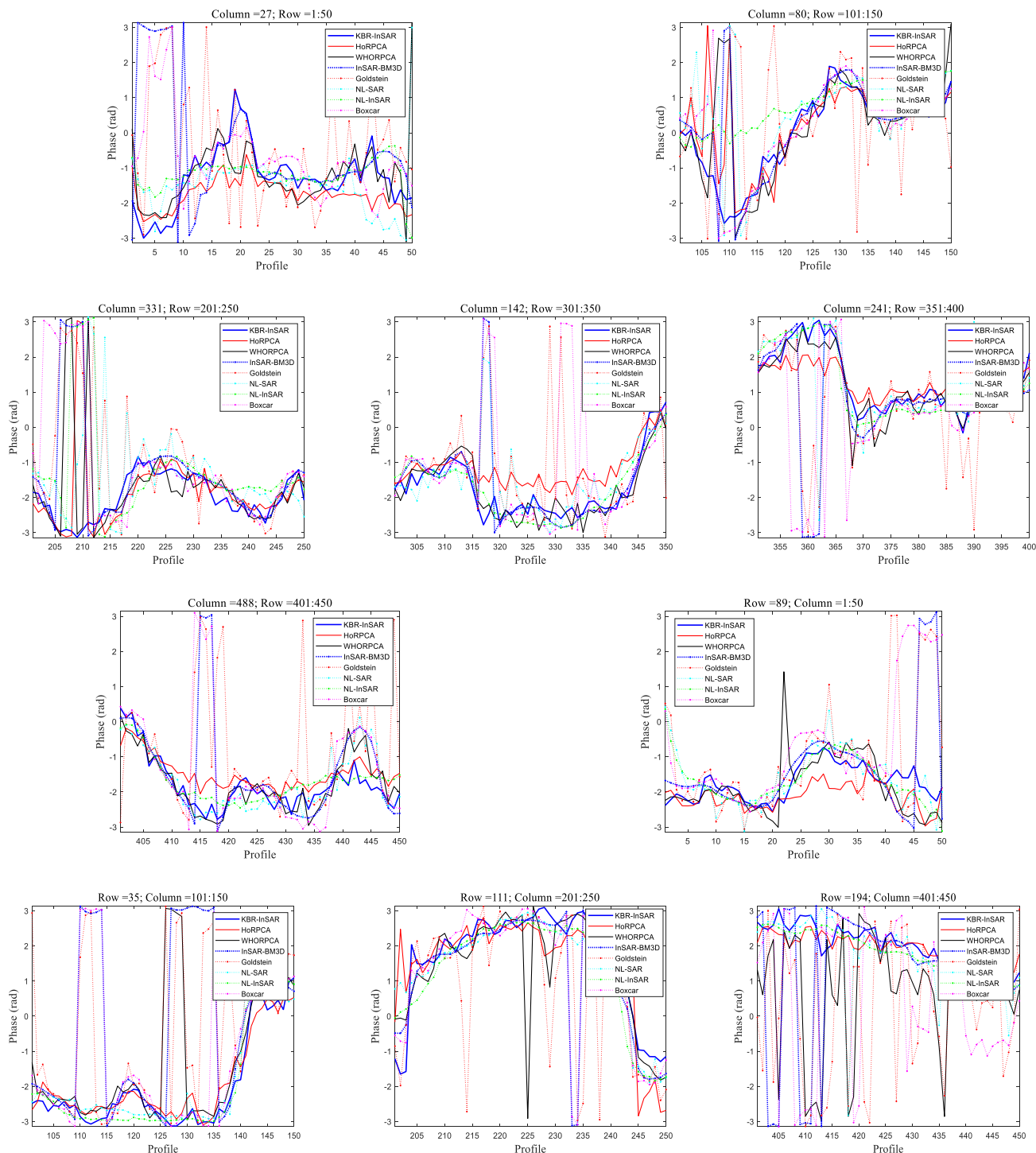
FIGURE 19. The filtered phase profiles (marked by white short line in Figure 18) with KBR-InSAR (blue dotted line) and other reference filtered methods. Although the filtered result of InSAR-BM3D is intuitively acceptable shown in Figure 15, there are many phase steps in its results. More or less, the same shortcoming exists in the results of WHoRPCA, Goldstein and Boxcar.

of improving accuracy through tensor depth. If the number of interferograms in InSAR stack data, i.e. the depth of tensor, continues to grow, the quality of the filtered result, acquired by KBR-InSAR, will be noticeably improved.

VIII. CONCLUSION

InSAR tensor is the mathematical model of the multi-pass interferometric stack data. The low rank tensor, acquired by the tensor decomposition method, achieves the noise reduction and fringes preservation. However, the main issue

for low-rank tensor estimation is the selection of tensor rank definition. This paper analyses different definitions of InSAR tensor rank, including Tucker rank, CP rank and KBR, and the feasibility of their application in interferometric phase filtering is discussed. Based on these analysis, KBR-InSAR is proposed to improve the performance of filtering in low SNR and solve the problem caused by over low-rank, which is established on KBR and an improved InSAR phase tensor model. Our improved InSAR phase tensor model further separates the outlier tensor into isolated phase jump-points caused by spatial under-sampling and Gaussian noise term, which supports the decomposition of InSAR tensor.

The experiments are conducted with simulated data and real InSAR stack data generated from Sentinel-1B. In the first simulated experiment, KBR-InSAR outperforms other tensor-based methods with various noisy conditions in terms of MSE of filtered results, which verify the robustness and practicability of KBR-InSAR. In the second simulated experiment, the performance of the proposed filter and other widespread filters are compared on the natural terrain and urban terrain with dense or sparse fringes, and quantitative and visual results demonstrate the superiority of our method. In the experiment on real data, the performance of these filters is outlined and the effectiveness of KBR-InSAR is proved.

REFERENCES

[1] L. Ying, D. C. Munson, R. Koetter, and B. J. Frey, "Multibaseline InSAR terrain elevation estimation: A dynamic programming approach," in *Proc. Int. Conf. Image Process.*, Sep. 2003, pp. 157–161.

[2] T. Wang, D. Perissin, M. S. Liao, and F. Rocca, "Deformation monitoring by long term D-InSAR analysis in three gorges area, China," in *Proc. IEEE IGARSS*, Jul. 2008, pp. 1–5.

[3] A. J. Roscoe and S. M. Blair, "Choice and properties of adaptive and tunable digital boxcar (moving average) filters for power systems and other signal processing applications," in *Proc. IEEE AMPS*, Sep. 2016, pp. 1–6.

[4] J.-S. Lee, "Refined filtering of image noise using local statistics," *Comput. Graph. Image Process.*, vol. 15, no. 4, pp. 380–389, 1981.

[5] W. Chen, H. Song, and X. Chuai, "Fully automatic random noise attenuation using empirical wavelet transform," *J. Seismic Explor.*, vol. 28, no. 2, pp. 147–162, Apr. 2019.

[6] W. Chen and S. Song, "Automatic noise attenuation based on clustering and empirical wavelet transform," *J. Appl. Geophys.*, vol. 159, pp. 649–665, Dec. 2018.

[7] R. M. Goldstein and C. L. Werner, "Radar interferogram filtering for geophysical applications," *Geophys. Res. Lett.*, vol. 25, no. 21, pp. 4035–4038, Nov. 1998.

[8] X. Lin, F. Li, D. Meng, D. Hu, and C. Ding, "Nonlocal SAR interferometric phase filtering through higher order singular value decomposition," *IEEE Trans. Geosci. Remote Sens. Lett.*, vol. 12, no. 4, pp. 806–810, Apr. 2015.

[9] C.-A. Deledalle, L. Denis, G. Poggi, F. Tupin, and L. Verdoliva, "Exploiting patch similarity for SAR image processing: The nonlocal paradigm," *IEEE Signal Process. Mag.*, vol. 31, no. 4, pp. 69–78, Jul. 2014.

[10] J. Hu, R. Guo, X. Zhu, G. Baier, and Y. Wang, "Non-local means filter for polarimetric SAR speckle reduction-experiments using TerraSAR-x data," *ISPRS Ann. Photogramm., Remote Sens. Spatial Inf. Sci.*, vol. 2, no. 3, pp. 71–77, 2015.

[11] A. Buades, B. Coll, and J.-M. Morel, "A non-local algorithm for image denoising," in *Proc. IEEE Comput. Soc. Conf. (CVPR)*, vol. 2, Jun. 2005, pp. 60–65.

[12] C.-A. Deledalle, L. Denis, and F. Tupin, "NL-InSAR: Nonlocal interferogram estimation," *IEEE Trans. Geosci. Remote Sens.*, vol. 49, no. 4, pp. 1441–1452, Apr. 2011.

[13] C.-A. Deledalle, L. Denis, F. Tupin, A. Reigber, and M. Jäger, "NL-SAR: A unified nonlocal framework for resolution-preserving (Pol)(In)SAR denoising," *IEEE Trans. Geosci. Remote Sens.*, vol. 53, no. 4, pp. 2021–2038, Apr. 2015.

[14] K. Dabov, A. Foi, V. Katkovnik, and K. Egiazarian, "Image denoising by sparse 3-D transform-domain collaborative filtering," *IEEE Trans. Image Process.*, vol. 16, no. 8, pp. 2080–2095, Aug. 2007.

[15] F. Sica, D. Cozzolino, X. X. Zhu, L. Verdoliva, and G. Poggi, "InSAR-BM3D: A nonlocal filter for SAR interferometric phase restoration," *IEEE Trans. Geosci. Remote Sens.*, vol. 56, no. 6, pp. 3456–3467, Jun. 2018.

[16] J. Kang, Y. Wang, M. Körner, and X. X. Zhu, "Robust object-based multipass InSAR deformation reconstruction," *IEEE Trans. Geosci. Remote Sens.*, vol. 55, no. 8, pp. 4239–4251, Aug. 2017.

[17] J. Kang, Y. Wang, M. Schmitt, and X. X. Zhu, "Object-based multipass InSAR via robust low-rank tensor decomposition," *IEEE Trans. Geosci. Remote Sens.*, vol. 56, no. 6, pp. 3062–3077, Jun. 2018.

[18] I. T. Jolliffe, *Principal Component Analysis*. Hoboken, NJ, USA: Wiley, 2002.

[19] E. J. Candès, X. Li, Y. Ma, and J. Wright, "Robust principal component analysis?" *J. ACM*, vol. 58, no. 3, p. 11, May 2011.

[20] T. G. Kolda and B. W. Bader, "Tensor decompositions and applications," *SIAM Rev.*, vol. 51, no. 3, pp. 455–500, 2009.

[21] D. Goldfarb and Z. Qin, "Robust low-rank tensor recovery: Models and algorithms," *SIAM J. Matrix Anal. Appl.*, vol. 35, no. 1, pp. 225–253, 2014.

[22] C. Lu, J. Feng, Y. Chen, W. Liu, Z. Lin, and S. Yan, "Tensor robust principal component analysis: Exact recovery of corrupted low-rank tensors via convex optimization," in *Proc. IEEE Conf. Comput. Vis. Pattern Recognit.*, Aug. 2017, pp. 5249–5257.

[23] Q. Xie, Q. Zhao, D. Meng, Z. Xu, S. Gu, W. Zuo, and L. Zhang, "Multispectral images denoising by intrinsic tensor sparsity regularization," in *Proc. IEEE CVPR*, Jun. 2016, pp. 1692–1700.

[24] J. Liu, P. Musialski, P. Wonka, and J. Ye, "Tensor completion for estimating missing values in visual data," *IEEE Trans. Pattern Anal. Mach. Intell.*, vol. 35, no. 1, pp. 208–220, Jan. 2013.

[25] M. Signoretto, Q. T. Dinh, L. De Lathauwer, and J. A. K. Suykens, "Learning with tensors: A framework based on convex optimization and spectral regularization," *Mach. Learn.*, vol. 94, no. 3, pp. 303–351, Mar. 2014.

[26] S. Gandy, B. Recht, and I. Yamada, "Tensor completion and low-n-rank tensor recovery via convex optimization," *Inverse Problems*, vol. 27, no. 2, Jan. 2011, Art. no. 025010.

[27] C. J. Hillar and L.-H. Lim, "Most tensor problems are NP-hard," *J. ACM*, vol. 60, no. 6, p. 45, Nov. 2009.

[28] A. Ferretti, C. Prati, and F. Rocca, "Permanent scatterers in SAR interferometry," *IEEE Trans. Geosci. Remote Sens.*, vol. 39, no. 1, pp. 8–20, Jan. 2001.

[29] A. Ferretti, C. Prati, and F. Rocca, "Non-uniform motion monitoring using the permanent scatterers technique," in *Proc. Eur. Space Agency (Special Publication)*, Jan. 2000, pp. 431–436.

[30] R. Tomioka, K. Hayashi, and H. Kashima, "Estimation of low-rank tensors via convex optimization," 2010, *arXiv:1010.0789*. [Online]. Available: https://arxiv.org/abs/1010.0789

[31] S. Boyd, N. Parikh, E. Chu, B. Peleato, and J. Eckstein, "Distributed optimization and statistical learning via the alternating direction method of multipliers," *Found. Trends Mach. Learn.*, vol. 3, no. 1, pp. 1–122, Jan. 2011.

[32] E. J. Candes, M. B. Wakin, and S. P. Boyd, "Enhancing sparsity by reweighted 1 minimization," *J. Fourier Anal. Appl.*, vol. 14, nos. 5–6, pp. 877–905, 2008.

[33] Y. G. Peng, J. L. Suo, Q. H. Dai, and W. L. Xu, "Reweighted low-rank matrix recovery and its application in image restoration," *IEEE Trans. Cybern.*, vol. 44, no. 12, pp. 2418–2430, Dec. 2014.

[34] M. Rup, L. K. Hansen, and S. M. Arnfred, "Algorithms for sparse nonnegative tucker decompositions," *Neural Comput.*, vol. 20, no. 8, pp. 2112–2231, Sep. 2008.

[35] Q. Xie, Q. Zhao, D. Meng, and Z. Xu, "Kronecker-basis-representation based tensor sparsity and its applications to tensor recovery," *IEEE Trans. Pattern Anal. Mach. Intell.*, vol. 40, no. 8, pp. 1888–1902, Aug. 2017.

YANAN YOU received the B.Sc. degree from the China University of Mining and Technology, in 2009, and the Ph.D. degree from the School of Electronic and Information Engineering, Beihang University, China, in 2015, where he held a Postdoctoral position, from 2015 to 2017. Since 2017, he has been a Lecturer with the School of Information and Communication Engineering, Beijing University of Posts and Telecommunications, China. His current research interests include SAR interferometry, deep learning image process, and big data technology.

RUI WANG received the bachelor's degree from the School of Information and Communication Engineering, Beijing University of Posts and Telecommunications, where she is currently pursuing the master's degree. Her research interests include SAR interferometry, deep learning image process, and computer vision.

WENLI ZHOU received the Ph.D. degree in signal and information processing from the Beijing University of Posts and Telecommunications, China, where he is currently an Associate Professor with the Broadband Network Monitoring Teaching and Research Center. His research interests include network traffic monitoring, user behavior analysis, and Internet big data processing.

• • •